Liquid–Solid Triboelectric Nanogenerator Arrays Based on Dynamic Electric-Double-Layer for Harvesting Water Wave Energy

Xi Liang, Shijie Liu, Shiquan Lin, Hongbo Yang, Tao Jiang,* and Zhong Lin Wang*

In the new energy era, ocean wave energy is recognized as one of the most important clean and renewable energy sources. As an advanced energy technology, developing triboelectric nanogenerators (TENGs) to harvest ocean wave energy has become a promising research direction. However, for most of the current fully enclosed TENGs or liquid–solid TENGs, the industrialization is limited. In this work, a TENG with a new working scheme is proposed for water wave energy harvesting. Through designing the opposite dynamic electric-double-layers, the efficient conversion of water kinetic energy into electrical energy is achieved. Moreover, the TENG structure is extended to an array. Under irregular water waves, the TENG array exhibits desired output performance, with the stable output current of 60.0 µA, output voltage of 60.0 V, and average power density of 5.38 W m^{-3}. Finally, the TENG array is demonstrated to successfully power signal spotlights, the digital thermometer and the water quality detector. This study not only broadens the research ideas for TENGs, but also provides a new mechanism for the ocean wave energy exploitation, which is of great significance to the industrialization of TENGs and blue energy.

1. Introduction

As an important clean and renewable energy source, the exploitation of ocean wave energy alleviates the energy crisis effectively, and will change all aspects of human production and life.[1,2] Triboelectric nanogenerator (TENG), which is an advanced energy harvesting technology invented by Wang in 2012,[3] has provided a promising route toward ocean wave energy development.[1,4–6] At this stage, most of the TENG devices adopt the fully enclosed mode.[6–11] However, the mechanical structures of these devices are usually too complicated to be manufactured, and the adaptability of the internal components with water waves is poor.[1,12–15] In addition, the contradiction between low wear of the materials and high performance of TENGs is difficult to balance.[16–19] More importantly, water leakage can have an irreversible damage to these devices, but the long-term stable waterproof packaging process still needs to be further verified.[20–22]

For all types of TENGs, the fundamental physics is based on the expanded Maxwell's displacement current, and its core is the included polarization density term P_s in electrical displacement vector, which is owing to electrostatic charges on the medium surfaces as produced by non-electric field effect such as triboelectrification.[23] When the charged mediums of TENGs are in contact with water, the interfacial interaction is dominated by electric-double-layers (EDLs).[24–26] The EDLs create strong electric fields and contain huge energy.[26] Recently, based on the EDL theory, electricity has been generated from various dynamic processes of water including flowing, waving, dropping and evaporating,[26–30] in the form of liquid–solid TENGs, droplet generators, evaporation generators or others. These methods can avoid the problems of fully enclosed TENGs for water wave energy harvesting, but the output performance is still relatively low now.[24,29,31,32]

In this work, a novel liquid–solid TENG with an asymmetric conuration was designed and fabricated to improve the capability of water wave energy harvesting. This TENG is based on the opposite dynamic EDLs and adopts a new working scheme, which is an innovation compared to previous fully enclosed TENGs and liquid–solid TENGs. First, we explored the typical output characteristics of the TENG in the pure water. By changing the liquid type and designing the micron-scale gap, the working principle of the TENG was carefully analyzed. Second, the output

X. Liang, S. Liu, S. Lin, H. Yang, T. Jiang, Z. L. Wang
CAS Center for Excellence in Nanoscience, Beijing Key Laboratory of
Micro-Nano Energy and Sensor, Beijing Institute of Nanoenergy and
Nanosystems
Chinese Academy of Sciences
Beijing 101400, P. R. China
E-mail: jiangtao@binn.cas.cn; zhong.wang@mse.gatech.edu
X. Liang, S. Liu, S. Lin, T. Jiang
School of Nanoscience and Engineering
University of Chinese Academy of Sciences
Beijing 100049, P. R. China
H. Yang
College of Engineering
Zhejiang Normal University
Jinhua 321004, P. R. China
Z. L. Wang
Georgia Institute of Technology
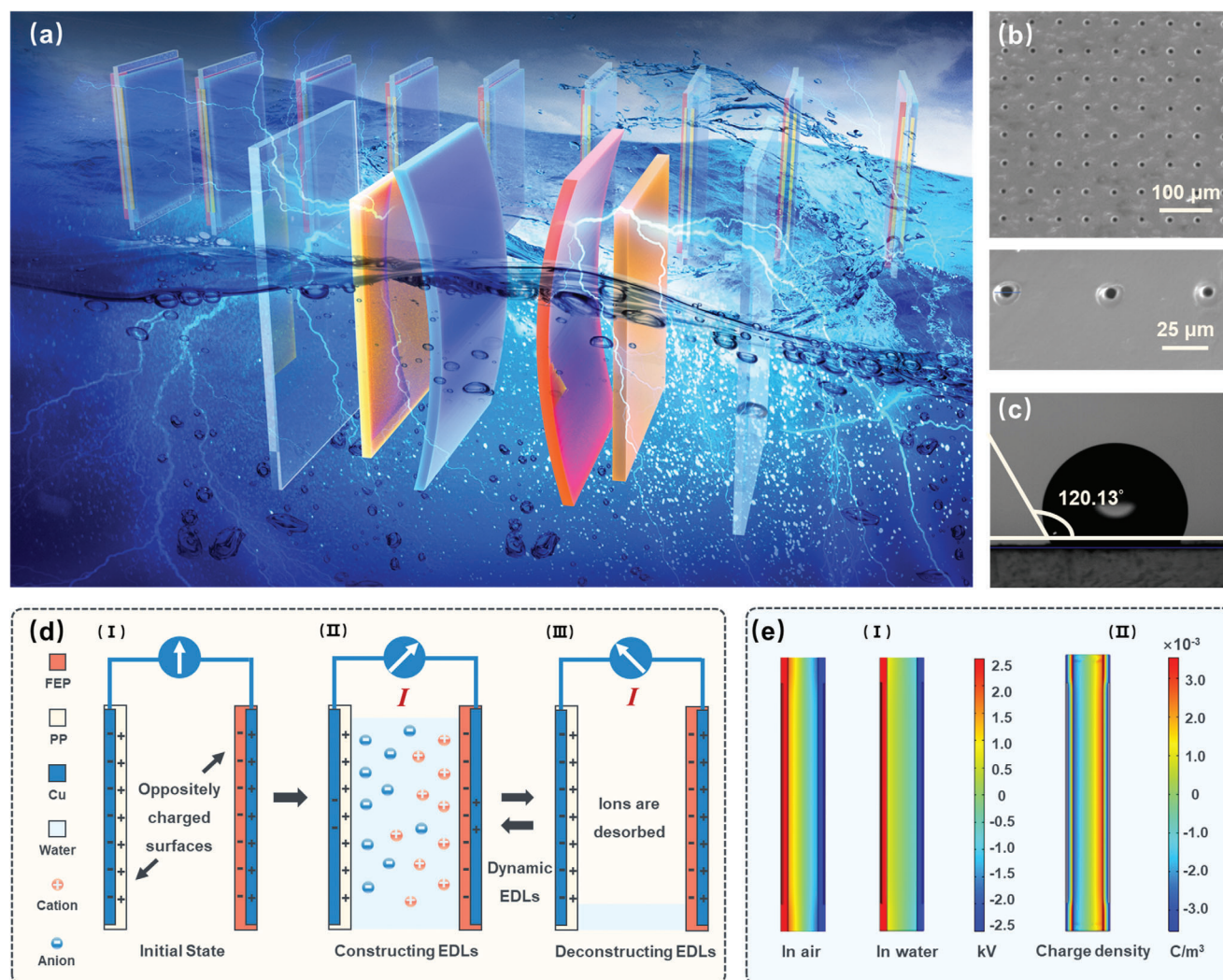Atlanta, GA 30332-0245, USA

Figure 1. a) Exploded view of the DE-TENG. b) SEM image of the treated FEP surface. c) Contact angle of the pure water with the treated FEP film. d) Working principle of the DE-TENG. e) Electric potential distributions of the DE-TENG in the air and in the water, and the charge density distribution in the water.

performance of the TENG under different working conditions was discussed in detail. The condition parameters include the liquid concentration, the motion frequency, and the motion height. Third, the TENG was extended into an array, and the TENG array was applied for the irregular water wave environment. Finally, the application potential of the TENG array was demonstrated. The signal spotlights, the digital thermometer, and the water quality detector were successfully powered. This work realizes the simple and efficient collection of the water wave energy, and provides new ideas for the industrialization of TENGs and blue energy, even for carbon neutrality.

2. Results and Discussion

The exploded view of the triboelectric nanogenerator based on the dynamic electric-double-layer (DE-TENG) is shown in **Figure 1**a, and the specific structure is shown in Figure S1 (Supporting Information). Two rectangular acrylic sheets (70 mm × 65 mm × 2 mm) were applied as the substrates of the DE-TENG, leaving a certain gap between them (gap width: 2 mm). The core of the DE-TENG is a polypropylene (PP) film and a fluorinated ethylene propylene (FEP) film with the same size (64 mm × 64 mm × 100 μm), and copper (Cu) electrodes (60 mm × 60 mm) were plated on the back of them by magnetron sputtering. The photographs of the two films with the electrodes are exhibited in Figure S2a (Supporting Information). Then, the two films were attached to the acrylic sheets and stood opposite each other, and water waves can undulate between them. According to the triboelectric series,[33,34] the FEP is more negative than water, while PP is similar to slippery nylon 66, which is relatively positive than water.[35] Therefore, the entire DE-TENG structure can be regarded as an asymmetric conuration, and the photograph from different angles are shown in Figure S2b,c (Supporting Information). In fact, as the positive triboelectric material, PP is not the best choice. However, the charges on the films of the DE-TENG must keep stable, and PP is a good electret material, which is the

ADVANCED
SCIENCE NEWS
www.advancedsciencenews.com

ADVANCED
ENERGY
MATERIALS
www.advenergymat.de

reason why other positive triboelectric materials cannot replace PP. Compared with most of the current fully enclosed TENG devices, the structure of this DE-TENG is simpler and easier to manufacture, and its volume is only 2.73×10^{-5} m³. Moreover, the DE-TENG structure is convenient to be extended into an array, and the conceptual diagram of the DE-TENG array is depicted in the background of Figure 1a.

Since the DE-TENG structure is open and works in the water environment, it is necessary to improve the hydrophobicity of the film surfaces. The method of inductively coupled plasma (ICP) etching was applied to construct microstructures on the film surfaces. The detailed process of the ICP etching is described in the Experimental Section. The upper image of Figure 1b displays the scanning electron microscopy (SEM) image of the treated FEP surface, presenting uniform microstructures distributed across the whole area. In the lower image of Figure 1b, the SEM image with a higher magnification further reveals that the diameter of a single protrusion is about 10 μm, and the spacing between each protrusion is 50 μm. In order to demonstrate the function of the microstructures, the contact angles of pure water with the original film and the treated film were measured. According to Figure S3 (Supporting Information) and Figure 1c, the microstructures increase the contact angle from 93.72° to 120.13°, illustrating that the hydrophobicity of the film surface is enhanced. For the PP film, the contact angle increases from 95.86° to130.76°, and Figure S4 (Supporting Information) exhibits the contact angles of the pure water with the original PP film and the treated PP film. With high hydrophobicity, water can slide quickly on the film surface with little residue, which is beneficial to the working efficiency of the DE-TENG.

The working process of the DE-TENG is demonstrated in Figure 1d. Before being placed in the water environment, the two film surfaces of the DE-TENG are first oppositely charged by contact electrification or other methods. Specifically, the PP film surface is positively charged, while the FEP film surface is negatively charged, which is indicated as the initial state (Figure 1d-I). When the DE-TENG is placed in the water environment, the device is submerged and the gap is filled with water (Figure 1d-II). The opposite electric-double-layers (EDLs) are formed in order to neutralize the surface potentials of the two films, causing free charges to flow in the external circuit through the back electrodes. As the water level drops below the device, the EDLs on the film surfaces deconstructs (Figure 1d-III). Correspondingly, the surface potentials tend to return to the original state, thus the free charges flow back. If water waves continue to rise and fall, the EDLs will be periodically constructed and deconstructed, forming dynamic boundary at the gas–liquid–solid interfaces, which are considered as dynamic EDLs. The dynamic EDLs can drive free charges to flow back and forth between the two electrodes, resulting in the alternating-current (AC) output of the DE-TENG. The above explains the mechanism of the DE-TENG working in water waves.

In order to reveal the working process, the corresponding electric potential distributions of the DE-TENG in the air and in the water were simulated by the finite element method. As shown in Figure 1e-I, compared with the air condition, the surface potentials of the two films in water are both decreased. In water, the opposite charges tend to accumulate at the interfaces of the films and the water. However, these accumulated charges can

only weaken the surface potentials, but not fully neutralize or reverse them, so the potential change is not very obvious. The specific potential curves were calculated in Figure S5 (Supporting Information). Respectively, Figure S5a (Supporting Information) is for the PP film, and Figure S5b (Supporting Information) is for the FEP film. With the DE-TENG submerged into the water, the potential on each surface drops by 120 V. Moreover, the charge density distribution of the DE-TENG in water was simulated in Figure 1e-II. It can be found that the opposite ions are attracted by the charged films, illustrating the formation of the EDLs.

Furthermore, the typical output characteristics of the DE-TENG were explored. For the purpose of regular testing, a special bracket was fabricated and connected to a vibration platform, which could drive the DE-TENG to move up and down in the water tank, and the schematic diagram is shown in Figure S6 (Supporting Information). During the operation, the DE-TENG keeps being intermittently submerged and emerged from the water. Taking one cycle as an example, the change of the water level relative to the DE-TENG device is presented in **Figure 2**a, and the corresponding transferred charge is shown in Figure 2b. Note that before being placed in the water environment, the PP film of the DE-TENG was positively polarized (5 kV, 5 min), and the FEP film was negatively polarized (−5 kV, 5 min). In addition, the pure water was applied, and the motion frequency and height were 0.5 Hz and 6 cm, ensuring that the DE-TENG can be fully submerged. When the DE-TENG is gradually submerged in water (the relative water level rises), the transferred charge increases from 0 to 0.44 μC. Next, the transferred charge curve rises by only 1.5 nC. Compared to the transferred charge of 0.44 μC in the entire process, this tiny uptrend can be negligible, which may be ascribed to inaccurate measurement and environmental disturbances. During this period, the transferred charge curve remains nearly stable, indicating that no charge is flowing in the circuit. When the DE-TENG is emerged from the water (the relative water level drops), the transferred charge decreases back to 0. As the relative water level rises and drops, this cycle is repeated, and the DE-TENG continues to output electricity.

For the purpose of verifying the output of the DE-TENG is derived from the dynamic EDLs, the output performances under the pure water and pure alcohol conditions were compared. As shown in Figure 2c, the transferred charge under the pure water condition is stable at 0.44 μC, but only 0.05 μC under the alcohol condition. Additionally, the output current and output voltage of DE-TENG under the pure water condition are exhibited in Figure S7a,b (Supporting Information). The average peak value of the output current is 2.2 μA, and the output voltage is 75.0 V. For the alcohol condition, the output current is 0.4 μA, and the output voltage is only 0.2 V, which are shown in Figure S8a,b (Supporting Information). Regardless of which parameter, the output performance under the water condition is significantly better than that of the alcohol condition. Compared with the water, the alcohol is an organic substance without any ions, so it is impossible to form EDLs. The small output of the DE-TENG under the alcohol condition may be due to its polarity. In Figure 2d, the dipole deflection of the alcohol under the action of the charged films are schematically illustrated. In summary, it can be deduced that the existence of the EDLs is the basis of the DE-TENG output.

On the other hand, we adjusted the gap width of the DE-TENG structure to demonstrate the role of the EDLs. When the gap
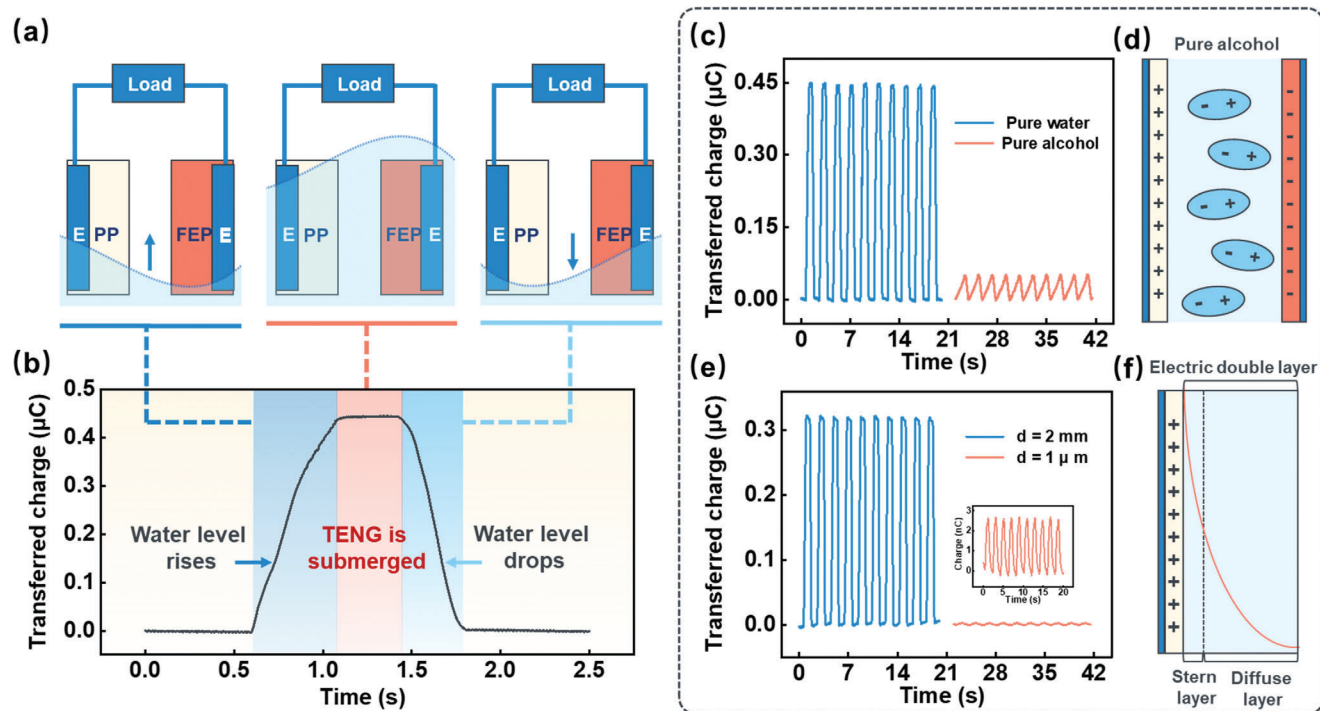
Figure 2. a) Schematic illustration for the change of the water level relative to the DE-TENG. b) Corresponding transferred charge of the DE-TENG in one cycle. c) Transferred charges of the DE-TENG under the pure water condition and the pure alcohol condition. d) Deflection of dipoles in the alcohol under the action of the charged films. e) Transferred charges of the DE-TENG with the gap width of 2 mm and 1 μm. f) Classical EDL structure at the interface of a charged surface and water.

width changes in the millimeter scale, the transferred charge of the DE-TENG is almost the same, as shown in Figure S9 (Supporting Information). In these conditions, the gap widths are much higher than the thickness of the EDLs (the Debye-length). Therefore, The EDLs at the two film surfaces do not affect each other, and the dynamic processes of the EDLs are similar. Generally, the Debye-length of solution is in the nanometer scale, but for the pure water without CO_2 dissolution, the Debye-length can reach 1 μm.[36] Then, a DE-TENG device with a gap width of 1 μm was fabricated by the method of film coating, and the detailed process is described in Figure S10 (Supporting Information) and the Experimental section. Under the distilled water condition, the transferred charges of the DE-TENG with the gap width of 2 mm and 1 μm are compared in Figure 2e. For the gap width of 2 mm, the transferred charge reaches 0.32 μC, while for the gap width of 1 μm, it is less than 3 nC. Figure S11a,b (Supporting Information) exhibits the output current and output voltage of the DE-TENG with the gap width of 1 μm, which are all at a very poor level. Due to the capillary effect, as the DE-TENG begins to be inserted into water, the water in the gap presents a convex surface, and the water level drops to compensate for the additional pressure. In order to fill the gap as much as possible, we submerged the DE-TENG at a deep position below the water surface, so that the water can cover the top of the device completely. In this case, the air bubbles in the gap can be expelled by water pressure, thus the capillary effect is not the key factor causing the decline in the output performance. This result can be explained by the EDL theory, which is proposed by Helmholtz in 1853, and Figure 2f shows the classical EDL structure at the interface of a charged surface and

water. The EDL is composed of an ion layer firmly adsorbed on the solid surface, known as the Stern layer, as well as the diffusion layer that can be easily influenced by applied external forces.[26] Therefore, the output of the DE-TENG mainly depends on the diffuse layer. When the gap width keeps much larger than the Debye-length, the schematic diagram of the DE-TENG immersed in water to form two opposite EDLs is described in Figure S12a (Supporting Information). Obviously, in this case, the EDLs at the two film surfaces can act independently. However, if the gap width becomes smaller than the Debye-length, the diffuse layers of the EDLs will be squeezed thin, which is indicated by the dotted line in Figure S12b (Supporting Information). Consequently, the output performance of DE-TENG with the gap width of 1 μm becomes very poor. This result also proves that the working process of the DE-TENG is derived from the dynamic EDLs.

In above experiments, the method of high-voltage polarization was adopted to inject charges to the two film surfaces in advance. In fact, besides this method, contact electrification is also an effective way to generate opposite charges on the two film surfaces. After the periodic contact-separation between the two films at the frequency of 1 Hz for 5 min, we assembled the DE-TENG device (gap width of 2 mm) and tested its output performance under the same condition as the previous experiments. Figure S13a–c (Supporting Information) are the output current, transferred charge and output voltage of the DE-TENG, illustrating the feasibility of this approach.

Moreover, in order to explain the advantages of the asymmetric conuration of the DE-TENG structure, we conducted two experiments for comparison. First, when only one film is utilized
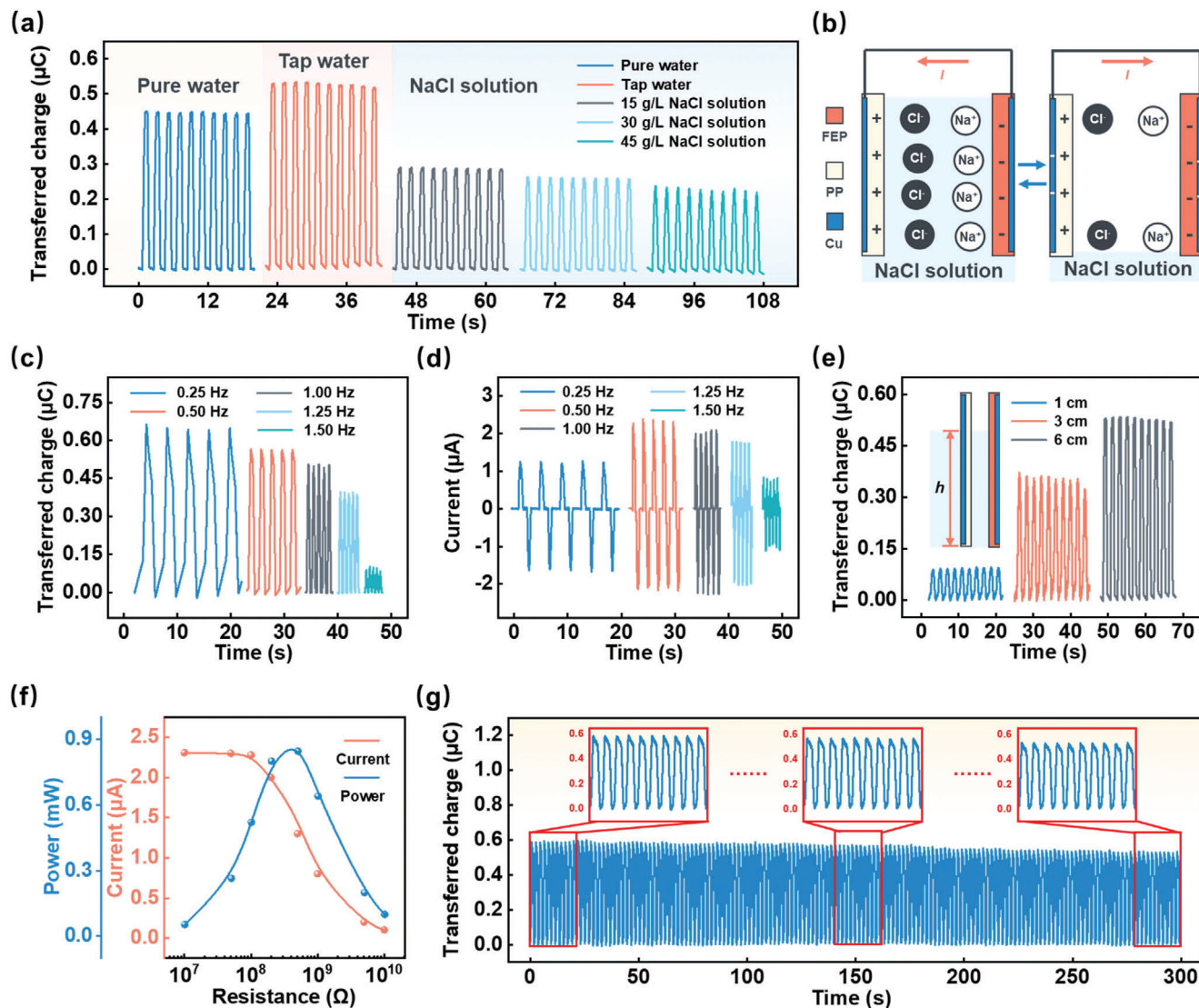
**ADVANCED
SCIENCE NEWS**

www.advancedsciencenews.com

**ADVANCED
ENERGY
MATERIALS**

www.advenergymat.de

Figure 3. a) Transferred charges of the DE-TENG in different liquid environments. b) Working process of the DE-TENG in the NaCl solutions. c) Transferred charges and d) output currents of the DE-TENG with the motion frequency increasing from 0.25 to 1.50 Hz. e) Transferred charges of the DE-TENG with the motion height increasing from 1 to 6 cm. f) Output current and power-resistance profiles of the DE-TENG under the optimal parameters. g) Transferred charge of the DE-TENG working in the tap water for 300 s.

and the electrode is grounded (Figure S14a, Supporting Information), which is consistent with the ordinary liquid–solid TENG, the transferred charge is shown in Figure S14b (Supporting Information). The charge transfer directions of the TENGs with the FEP film and the PP film are opposite, and both are smaller than the DE-TENG, proving that the introduction of the two films is effective. Then, when FEP films are applied for both parts (Figure S14c, Supporting Information), the TENG outputs almost no power (Figure S14d, Supporting Information), because the potentials of the two electrodes are always the same. This result further suggests that the asymmetric conuration is necessary for the DE-TENG.

Subsequently, the influences of working conditions on the output performance of the DE-TENG were systematically investigated. In **Figure 3**a, the transferred charges of the DE-TENG in different liquid environments are shown, keeping the motion frequency at 0.5 Hz and the motion height at 6 cm. Compared with pure water, under the tap water condition, the transferred charge of the DE-TENG is larger, reaching 0.56 µC. The output current and output voltage under the tap water condition were measured, as shown in Figure S15a,b (Supporting Information). For the tap water in Beijing, calcium ions are the most important impurities, and the concentration is about 300 mg L^{-1}. The performance improvement is due to the presence of more ions in the tap water. Nevertheless, for the NaCl solutions, the output performance of the DE-TENG is worse than the result under the pure water, illustrating that the effect of the ion concentration on the output performance is not linear. Here, in order to match the salinity of general seawater, NaCl solutions with concentrations of 15, 30, and 45 g L^{-1} were applied. The ion concentrations of

**ADVANCED
SCIENCE NEWS**

www.advancedsciencenews.com

**ADVANCED
ENERGY
MATERIALS**

www.advenergymat.de

these solutions are much higher relative to the tap water, which affects the working process of the DE-TENG, as expressed in Figure 3b. In the high-concentration solution, more Na^+ and Cl^- are tightly bound on the film surfaces, and correspondingly, there are few ions that can escape from the film surfaces, leading to the decrease in the output performance. Figure S16a,b (Supporting Information) exhibits the output current and output voltage of the DE-TENG working under the 45 g L^{-1} NaCl solution. Although the adverse effect of the high ion concentration is unavoidable, the output performance of the DE-TENG in the NaCl solution like seawater still maintains at a certain level. Therefore, toward ocean wave energy harvesting, the program of the DE-TENG has application prospects.

Besides the solution concentration, the effect of polarization conditions on the output performance of the DE-TENG is also investigated. In this work, the distance between the tip of the high-voltage polarimeter and the films was kept at 1 cm. Generally, a higher applied voltage is beneficial to the polarization effect for films. At the distance of 1 cm, 5 kV is the highest voltage ensuring that the material will not be broken, thus the voltage value of 5 kV was applied here. As for the applied time of the high voltage, the transferred charge of the DE-TENG with the processing durations of 1, 2, 5, and 10 min was measured, which is shown in Figure S17 (Supporting Information). As can be seen, the longer time increases the output performance, but the result of 10 min is not improved significantly compared to 5 min. Therefore, the applied time of 5 min was selected here.

Moreover, the motion frequency and height are also two important factors to influencing the working efficiency of the DE-TENG. Here, the tap water and the polarization conditions of 5 kV, 5 min were adopted. With the motion frequency increasing from 0.25 Hz to 1.50 Hz (motion height $h = 6$ cm), the transferred charge of the DE-TENG is shown in Figure 3c. At the lower motion frequency, the contact time of the DE-TENG and water is longer, and the ion absorption is more sufficient. Therefore, with increasing the motion frequency, the transferred charge decreases gradually. Different from this trend, the output current in Figure 3d first rises and then falls, reaching the maximum value of 2.4 µA at 0.5 Hz. This is because the current is the derivative of the transferred charge with respect to time. Then, the influence of the motion height was investigated, fixing the motion frequency at 0.5 Hz. The motion height determines the maximum depth that the DE-TENG can be submerged, which is indicated in the inset of Figure 3e. As the motion height increases, the contact area of the DE-TENG and the water becomes larger, leading to more absorbed ions. According to Figure 3e and Figure S18 (Supporting Information), it can be analyzed that the higher motion height is beneficial to the output performance of the DE-TENG. Under the optimal working condition, where the motion frequency is at 0.5 Hz, and the motion height is at 6 cm, the output current and power-resistance profiles were measured in Figure 3f. The maximum of the peak power is 0.85 mW at the matched resistance of 500 MΩ, and the average power is 0.14 mW. In Figure S19 (Supporting Information), the peak power density was calculated to be 30.95 W m^{-3}, and the average power density reached 4.94 W m^{-3}. Moreover, the durability of the DE-TENG working in the water environment was explored. As shown in Figure 3g, after 300 s, the transferred charge of the DE-TENG decreases slightly, mainly due to the following

two points. On the one hand, even if the film surfaces have been treated hydrophobically, it is impossible to avoid the residual ions completely. On the other hand, for the electret film materials applied in the DE-TENG, a part of polarized charges existing on the film surfaces are not stable. Although the transferred charge declines slightly after 300 s, the DE-TENG still maintains a normal working state, illustrating its ability to work in the water environment for a long time.

On the basis of the single DE-TENG, multiple units were integrated to fabricate a DE-TENG array. **Figure 4**a shows the photograph of the DE-TENG array with 10 units, and the inset is the photograph from another angle. The entire DE-TENG array is quite small in size, only 2.47×10^{-4} m^3. For the circuit connection, the rectifier bridges were introduced to connect the units together in parallel, because it is impossible to completely unify the water movement in each unit, and the circuit diagram is shown in Figure 4b. With the unit number increasing from 1 to 10, the output currents of the DE-TENG array are compared in Figure 4c, fixing the working conditions consistent with the previous optimal parameters. For each DE-TENG unit, the output performance is at the same level, but it cannot be strictly controlled without any deviation. Owing to small differences between each unit, the output current of the array with 10 units is not exactly twice that of the array with 5 units. When 10 units are integrated, the output current reaches 23.4 µA. Because of the introduction of the rectifier bridges, the negative current peak was converted into another positive peak, presenting two positive current peaks. By integration, the transferred charge corresponding to a current peak was calculated as 4.57 µC, which is shown in Figure 4d. Accordingly, the transferred charge curve becomes the pattern of two rising steps. Figure S20 (Supporting Information) reveals the output voltage of the DE-TENG array with 10 units. Then the output current and power-resistance profiles were measured in Figure 4e. The maximum peak power of 4.05 mW is achieved at the matched resistance of 50 MΩ, and the corresponding average power is 0.68 mW. In Figure S21 (Supporting Information), the maximum peak power density is 16.4 W m^{-3}, and the average power density reaches 2.75 W m^{-3}. In addition, to evaluate the charging ability of the DE-TENG array, the charging curves for a series of capacitors from 10 to 470 µF are summarized in Figure 4f.

All of the above experiments were tested under the regular triggers, and it is necessary to estimate the output characteristics of the DE-TENG array driven by irregular water waves for its practical applications. Thus, we set the DE-TENG array on a wall of a water tank, and the bottom of the DE-TENG array is set close to the water surface. A series of wave pumps were applied to generate irregular water waves, and the wave frequency and height are about 2 Hz and 3 cm, respectively. Figure 4g,h shows the typical output current and output voltage of the DE-TENG array. As can be seen, the output peaks are very dense, since the water level in the gap of each unit continues to fluctuate, which are superior to the pulse signals of ordinary TENGs.[3] The output current reaches 60.0 µA, and the output voltage reaches 60.0 V. Besides, the output current and power-resistance relationships are shown in Figure 4i. The maximum peak power reaches 5.12 mW with the matched resistance of 5 MΩ, and the average power is 1.33 mW. In Figure S22 (Supporting Information), the maximum peak power density was calculated to be 20.73 W m^{-3},

**ADVANCED
SCIENCE NEWS**

www.advancedsciencenews.com
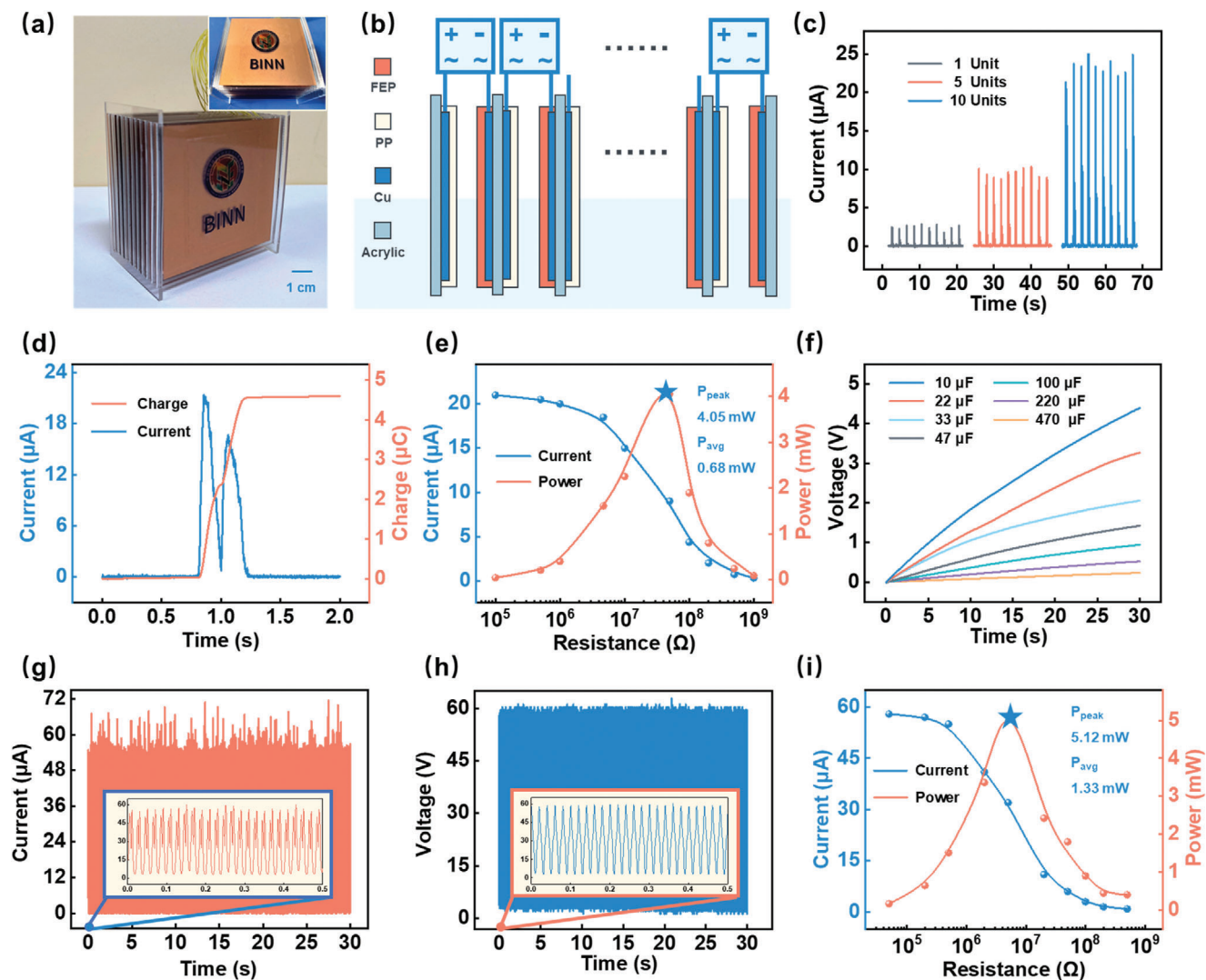
**ADVANCED
ENERGY
MATERIALS**

www.advenergymat.de

Figure 4. a) Photographs of the DE-TENG array with 10 units from two different angles. b) Circuit connection diagram of the DE-TENG array. c) Output currents of the DE-TENG array with the unit number increasing from 1 to 10. d) Transferred charge of the DE-TENG array corresponding to a current peak. e) Output current and power-resistance profiles of the DE-TENG array. f) Voltage curves for a series of capacitors from 10 to 470 µF charged by the DE-TENG array. g) Output current and h) output voltage of the DE-TENG array under the irregular water waves. i) Output current and power-resistance profiles of the DE-TENG array under the irregular water waves.

and the average power density is 5.38 W m^{-3}.[6] The peak power density of the DE-TENG array is compared with that of several typical TENG networks in previous papers in Figure S23 (Supporting Information),[21,37–40] illustrating that the output performance reaches a higher level. Note that no power management or any energy improvement schemes were introduced in this work.

Based on the powerful water wave energy harvesting capability of the DE-TENG array, its practical applications on powering portable electronics were demonstrated. **Figure 5**a is the schematic diagram of a large-scale DE-TENG array applied to the ocean scene. The DE-TENG array is built on the coast at the height of the ocean surface, converting the ocean wave energy into electrical energy to light up the street lamps along the coastal road. In this concept, the DE-TENG array consists of thousands of units, and here the DE-TENG array with 10 units is shown in

Figure 5b,c, which is only a small part of the envisioned array. The fabricated DE-TENG array was placed on the wall of the water tank, and the tap water was employed here for convenience. Figure 5b,c are the photographs of the stationary state and the wave state, respectively. Above all, the DE-TENG array was utilized to power three signal spotlights of red, yellow and green. The relevant photograph is exhibited in Figure 5d, and the experiment process was recorded in Video S1 (Supporting Information). Since the output peaks of the DE-TENG array are quite dense under irregular waves, the spotlights were continuously lit without flickers.

In order to accommodate more applications, the introduction of capacitors is inevitable. The voltage curves for capacitors from 10 to 470 µF charged by the DE-TENG array under irregular water waves were measured in Figure 5e. With a capacitor of 47 µF, the DE-TENG array successfully drove the digital
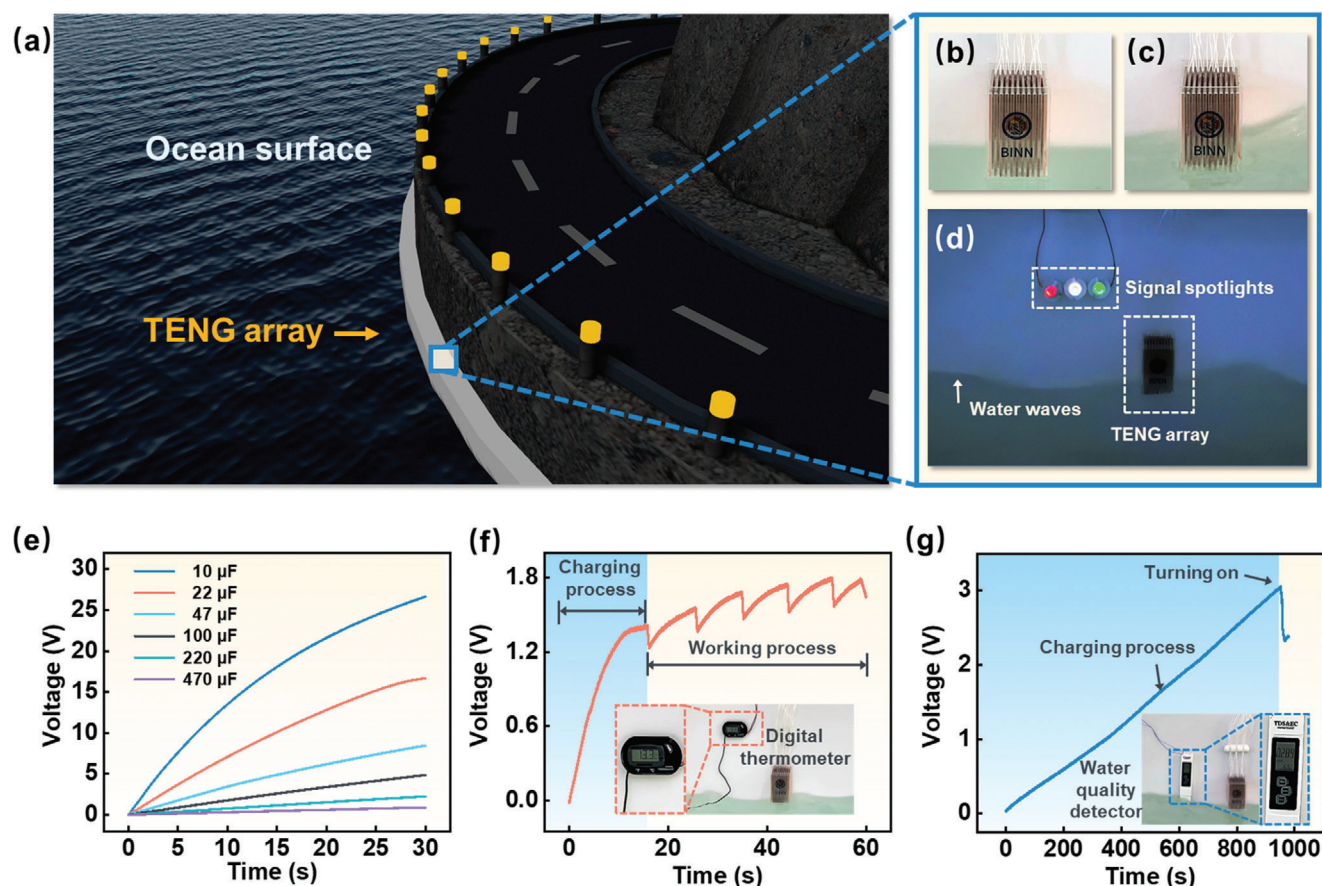
**ADVANCED
SCIENCE NEWS**

www.advancedsciencenews.com

**ADVANCED
ENERGY
MATERIALS**

www.advenergymat.de

Figure 5. a) Schematic diagram of a large-scale DE-TENG array applied to the ocean scene. b) Photograph of the DE-TENG array under the stationary state. c) Photograph of the DE-TENG array under the wave state. d) Photograph of the DE-TENG array powering three signal spotlights of red, yellow, and green. e) Voltage curves for capacitors from 10 to 470 µF charged by the DE-TENG array under the irregular water waves. Voltage curves on f) the digital thermometer and g) the water quality detector powered by the DE-TENG array.

thermometer to work, and Figure 5f shows the voltage curve of the working process. After the charging process of 15.75 s, the digital thermometer is automatically turned on, and then the temperature value is displayed on the screen, which is shown in the inset of Figure 5f. Note that the voltage curve always maintains the overall upward trend, implying that the thermometer can work constantly with water waves, and no additional charging process is required. The detailed working process is provided in Video S2 (Supporting Information). Furthermore, the water quality detector was applied as another application demonstration. Figure 5g is the voltage curve of the DE-TENG array charging a capacitor of 2.2 mF and powering the water quality detector. After the charging process of 950.65 s, the voltage value exceeds 3 V, which is the working voltage of the water quality detector. At this time, a mechanical switch is turned on, and the electrical energy stored in the capacitor is released to power the water quality detector. The inset in Figure 5g is the photograph of the water quality detector displaying the information, and the related experiment process is shown in Video S3 (Supporting Information). For better presentation, the photographs of the DE-TENGs powering the digital thermometer and the water quality detector are enlarged in Figure S24 (Supporting Information).

3. Conclusion

In this work, we designed and fabricated a unique asymmetric TENG with a new working scheme for water wave energy harvesting. With water movement, the opposite dynamic electric-double-layers at the two different film surfaces were proven to be the working basis of the TENG. The influences of various working conditions on its output performance were systematically investigated. Under the optimal parameters, the peak power density reaches 30.95 W m^{-3}, and the average power density reaches 4.94 W m^{-3}. Furthermore, the TENG units were integrated into an array, and it was placed in irregular water waves for testing. The output current of 60.0 µA and output voltage of 60.0 V were achieved, and the output peaks are quite dense and stable. The peak power density of the TENG array reaches 20.73 W m^{-3}, and the corresponding average power density is 5.38 W m^{-3}. Based on this desired output performance, the applications of the TENG were demonstrated. The TENG array was utilized to power signal spotlights, a digital thermometer and a water quality detector. In conclusion, we proposed a TENG with a new working scheme based on the dynamic EDLs for water wave energy harvesting, which improves the energy harvesting efficiency and provides new development idea for TENGs and blue energy.

4. Experimental Section

Fabrication of the DE-TENG Device: First, by magnetron sputtering (Discovery635), copper electrodes (60 mm × 60 mm) were plated on the PP film and FEP film (64 mm × 64 mm × 100 µm). Second, with a metal template, the surfaces of the film materials were modified by ICP etching (SI500) to construct microstructures. The etching time was 200 s, and the reaction gas was 15.0 sccm Ar, 10.0 sccm O_2 and 30.0 sccm CF_4. The surface morphology of the samples was characterized by SEM (NOVA200). The contact angles of the film and water were acquired by a contact angle measuring machine (XG-CAVB1). Third, two rectangular acrylic sheets (70 mm × 65 mm × 2 mm) were applied as the substrate of the DE-TENG. Fourth, utilizing the waterproof tape, the electrode-coated sides of the films were tightly attached to the two acrylic sheets. Finally, the two acrylic sheets were separated by two narrow acrylic strips of 2 mm or others in the thickness, and then they were combined into a whole by the acrylic glue, keeping a certain gap width. Through the above steps, a DE-TENG device was made.

Fabrication of the DE-TENG Device with a Gap Width of 1 µm: First, the films were modified and coated with electrodes, and then attached to the acrylic sheets, which is consistent with the previous steps. Second, a vacuum coating machine (BEVS 1811/3) was applied to coat PVA glue on the PP film surface to a thickness of 1 µm. Third, the FEP film and the PP film were combined and fixed together, and then dried for 12 h. Finally, the device was placed in the water environment, and the PVA was dissolved by water. In this way, a DE-TENG with a gap width of 1 µm was fabricated.

Fabrication of the DE-TENG Array: First, a series films were modified and coated with electrodes, and then they were adhered alternately on both sides of the acrylic sheets. For a TENG array with 10 units, 11 acrylic sheets were required. Then, another two acrylic sheets (47 mm × 75 mm × 2 mm) with 11 corresponding card slots were fabricated, and each slot had an interval of 2 mm. Finally, these 11 acrylic sheets were regulated through these slots, forming a DE-TENG array.

Electric Measurements of the DE-TENG Device: The regular triggers for the DE-TENG were provided by a vibration platform (NJLJ-6D(R)-60) with a special bracket. For the irregular water waves, a series of wave pumps (YHX 021) were set at the inner walls of a water tank to generate water waves. The output current, output voltage, and transferred charge of the TENG device were measured by a current preamplifier (Keithley 6514 System Electrometer), while the voltage after rectification was measured by a digital oscilloscope (Agilent InfiniiVision 2000X).

Supporting Information

Supporting Information is available from the Wiley Online Library or from the author.

Acknowledgements

Conflict of Interest

The authors declare no conflict of interest.

Data Availability Statement

The data that support the findings of this study are available from the corresponding author upon reasonable request.

[1] B. Huang, P. Wang, L. Wang, S. Yang, D. Wu, *Nanotechnol. Rev.* **2020**, *9*, 716.
[2] J. P. Painuly, *Renewable Energy* **2001**, *24*, 73.
[3] F. R. Fan, Z. Q. Tian, Z. L. Wang, *Nano Energy* **2012**, *1*, 328.
[4] Z. L. Wang, T. Jiang, L. Xu, *Nano Energy* **2017**, *39*, 9.
[5] T. Zhao, M. Xu, X. Xiao, Y. Ma, Z. Li, Z. L. Wang, *Nano Energy* **2021**, *88*, 106199.
[6] X. Liang, S. Liu, H. Yang, T. Jiang, *Electronics* **2023**, *12*, 225.
[7] H. Wang, L. Xu, Z. Wang, *Nanoenergy Adv.* **2021**, *1*, 32.
[8] M. Xu, T. Zhao, C. Wang, S. L. Zhang, Z. Li, X. Pan, Z. L. Wang, *ACS Nano* **2019**, *13*, 1932.
[9] S. Liu, X. Liang, P. Chen, H. Long, T. Jiang, *Small Methods* **2023**, *7*, 2201392.
[10] I. M. Imani, B. Kim, X. Xiao, N. Rubab, B. J. Park, Y. J. Kim, P. Zhao, M. Kang, S. W. Kim, *Adv. Sci.* **2023**, *10*, 2204801.
[11] R. Hinchet, H. Yoon, H. Ryu, M. Kim, E. Choi, D. Kim, S. Kim, *Science* **2019**, *365*, 491.
[12] H. Chen, C. Xing, Y. Li, J. Wang, Y. Xu, *Sustainable Energy Fuels* **2020**, *4*, 1063.
[13] R. Li, Y. Li, Y. Zhao, Y. Li, Y. Li, *Appl. Phys. Rev.* **2018**, *5*, 031303.
[14] C. Rodrigues, D. Nunes, D. Clemente, N. Mathias, J. M. Correia, P. Rosa-Santos, F. Taveira-Pinto, T. Morais, A. Pereira, J. Ventura, *Environ Sci* **2020**, *13*, 2657.
[15] W. Liu, L. Xu, T. Bu, H. Yang, G. Liu, W. Li, Y. Pang, C. Hu, C. Zhang, T. Cheng, *Nano Energy* **2019**, *58*, 499.
[16] Z. Lin, B. Zhang, H. Guo, Z. Wu, H. Zou, J. Yang, Z. L. Wang, *Nano Energy* **2019**, *64*, 103908.
[17] Z. Lin, B. Zhang, Y. Xie, Z. Wu, J. Yang, Z. L. Wang, *Adv. Funct. Mater.* **2021**, *31*, 2105237.
[18] Y. Feng, T. Jiang, X. Liang, J. An, Z. L. Wang, *Appl. Phys. Rev.* **2020**, *7*, 021401.
[19] Y. Feng, X. Liang, J. An, T. Jiang, Z. L. Wang, *Nano Energy* **2021**, *81*, 105625.
[20] S. Tian, X. Wei, L. Lai, B. Li, Z. Wu, Y. Dai, *Nano Energy* **2022**, *102*, 107669.
[21] X. Yang, L. Xu, P. Lin, W. Zhong, Y. Bai, J. Luo, J. Chen, Z. L. Wang, *Nano Energy* **2019**, *60*, 404.
[22] Z. Yuan, C. Wang, J. Xi, X. Han, J. Li, S.-T. Han, W. Gao, C. Pan, *ACS Energy Lett.* **2021**, *6*, 2809.
[23] Z. L. Wang, *Mater. Today* **2022**, *52*, 348.
[24] M. Xu, S. Wang, S. L. Zhang, W. Ding, P. T. Kien, C. Wang, Z. Li, X. Pan, Z. L. Wang, *Nano Energy* **2019**, *57*, 574.
[25] F. Zhan, A. C. Wang, L. Xu, S. Lin, J. Shao, X. Chen, Z. L. Wang, *ACS Nano* **2020**, *14*, 17565.
[26] Z. Zhang, X. Li, J. Yin, Y. Xu, W. Fei, M. Xue, Q. Wang, J. Zhou, W. Guo, *Nat. Nanotechnol.* **2018**, *13*, 1109.
[27] J. Tan, X. Wang, W. Chu, S. Fang, C. Zheng, M. Xue, X. Wang, T. Hu, W. Guo, *Adv. Mater.* **2023**, *35*, 2211165.
[28] J. K. Moon, J. Jeong, D. Lee, H. K. Pak, *Nat. Commun.* **2013**, *4*, 1487.
[29] L. Li, S. Feng, Y. Bai, X. Yang, M. Liu, M. Hao, S. Wang, Y. Wu, F. Sun, Z. Liu, T. Zhang, *Nat. Commun.* **2022**, *13*, 1043.

**ADVANCED
SCIENCE NEWS**

www.advancedsciencenews.com

**ADVANCED
ENERGY
MATERIALS**

www.advenergymat.de

[30] X. Huangfu, Y. Guo, S. M. Mugo, Q. Zhang, *Small* **2023**, e2207134.

[31] G. Zhu, Y. Su, P. Bai, J. Chen, Q. Jing Q, W. Yang, Z. L. Wang, *ACS Nano* **2014**, *8*, 6031.

[32] Q. Zhou, B. Wang, A. Gao, W. Xu, K. Zhou, J. Pan, G. Meng, C. Pan, F. Xia, *Adv. Funct. Mater.* **2022**, *32*, 2209100.

[33] H. Zou, L. Guo, H. Xue, Y. Zhang, X. Shen, X. Liu, P. Wang, X. He, G. Dai, P. Jiang, H. Zheng, B. Zhang, C. Xu, Z. L. Wang, *Nat. Commun.* **2020**, *11*, 2093.

[34] H. Zou, Y. Zhang, L. Guo, P. Wang, X. He, G. Dai, H. Zheng, C. Chen, A. C. Wang, C. Xu, Z. L. Wang, *Nat. Commun.* **2019**, *10*, 1427.

[35] Z. Wang, A. Berbille, Y. Feng, S. Li, L. Zhu, W. Tang, Z. L. Wang, *Nat. Commun.* **2022**, *13*, 130.

[36] Y. Wang, S. R. Narayanan, W. Wu, *ACS Nano* **2017**, *11*, 8421.

[37] X. Liang, T. Jiang, G. Liu, T. Xiao, L. Xu, W. Li, F. Xi, C. Zhang, Z. L. Wang, *Adv. Funct. Mater.* **2019**, *29*, 1807241.

[38] L. Xu, T. Jiang, P. Lin, J. J. Shao, C. He, W. Zhong, X. Y. Chen, Z. L. Wang, *ACS Nano* **2018**, *12*, 1849.

[39] T. Xiao, X. Liang, T. Jiang, L. Xu, J. Shao, J. Nie, Y. Bai, W. Zhong, Z. L. Wang, *Adv. Funct. Mater.* **2018**, *28*, 1802634.

[40] X. Liang, T. Jiang, Y. Feng, P. Lu, J. An, Z. L. Wang, *Adv. Energy Mater.* **2020**, *10*, 2002123.